Analysis of Markers for Combustion Mode and Heat Release in MILD Combustion Using DNS Data

N.A.K Doan* and N. Swaminathan

Department of Engineering, University of Cambridge, Cambridge, CB2 1PZ, UK.

*Corresponding author:
Currently at Technical University of Munich
E-mail: doan@tfd.mw.tum.de

(Draft to Combust. Sci. Technol. Special issue on UKCTRF workshop 2018)

Abstract

Various commonly used markers for heat release are assessed using direct numerical simulation (DNS) data for Moderate or Intense Low-oxygen Dilution (MILD) combustion to find their suitability for non-premixed MILD combustion. The laser induced fluorescence (LIF) signals of various markers are synthesised from the DNS data to construct their planar (PLIF) images which are compared to the heat release rate images obtained directly from the DNS data. The local OH values in heat releasing regions are observed to be very small compared to the background level coming from unreacted mixture diluted with exhaust gases. Furthermore, these values are very much smaller compared to those in burnt regions. This observation rises questions on the use of OH-PLIF for MILD combustion. However, the chemiluminescent image obtained using OH^* is shown to correlate well with the heat release. Two-scalar based PLIF markers, $(\mathrm{OH} \times \mathrm{CH_2O})$ and $(\mathrm{H} \times \mathrm{CH_2O})$, correlate well with the heat release. Flame index (FI) and chemical explosive mode (CEMA) analyses are used to identify premixed and non-premixed regions in MILD combustion. Although there is some agreement between the CEMA and FI results, large discrepancies are still observed. The schlieren images deduced from the DNS data showed that this technique can be used for a quick and qualitative identification of MILD combustion before applying expensive laser diagnostics.

Keywords: Direct Numerical Simulation (DNS), MILD combustion, PLIF-signal, heat release rate marker, schlieren

1 Introduction

Considerable progress has been made since 1980s on turbulence-combustion interaction, turbulent combustion modelling (Pope, 2013) and large eddy simulations of reacting flows in practical engines with complex geometries (Menon, 2018). This advancement has helped to find effective solutions to improve the engine efficiency, reduce pollutants emission and thereby to find ways to design "greener" combustion devices which are friendlier to the environment. Among potential green combustion modes, MILD combustion has gained significant attention because of its ability to reduce pollutants emission and increase efficiency (Wünning & Wünning, 1997; Cavaliere & de Joannon, 2004). The efficiency gain comes from the energy recovered by recirculating hot gases and the emission reduction is because of the reduced temperature rise and oxygen level in the combustion zone. This mode of combustion is said to occur when the reactant temperature, T_r, is higher than the reference auto-ignition temperature, T_{ign}, for a given fuel-air mixture and the temperature rise, $\Delta T = (T_p - T_r)$, is smaller than T_{ign} (Cavaliere & de Joannon, 2004). These two conditions are typically achieved by diluting the fuel-air mixture with exhaust gases so that the oxygen level is typically below 5% by volume.

The physics of MILD combustion is quite challenging to unravel because of the strong role of chemical kinetics. It was shown to have specific features such as the absence of a visible flame and spatially distributed heat release resulting in homogeneous temperature fields, which are atypical of conventional turbulent combustion (Ozdemir & Peters, 2001; Katsuki & Hasegawa, 1998; de Joannon *et al.*, 2000; Minamoto & Swaminathan, 2014; Sorrentino *et al.*, 2016). Indeed, conventional combustion has radicals such as OH concentrated in thin regions with large heat release rate (HRR) leading to strong gradients. Many past studies demonstrated that the HRR structures in premixed and non-premixed conventional combustions can be discerned using laser diagnostics (Nguyen & Paul, 1996; Paul & Najm, 1998; Balachandran *et al.*, 2005; Fayoux *et al.*, 2005; Tana-

hashi *et al.*, 2005; Kiefer *et al.*, 2009; Richter *et al.*, 2005; Li *et al.*, 2010; Rosell *et al.*, 2017). However, the applicability of these diagnostics to combustion under MILD conditions is unclear since the heat releasing regions in MILD combustion appear different from those in conventional combustion. Furthermore, radicals such as OH, CH and HCO used commonly as HRR markers are present in unreacted mixture of MILD combustion because of dilution using exhaust gases containing these species. Since the temperature rise across the reaction zones in MILD combustion is typically small, the increase in these radicals level above their background (non-reacting mixture) values may be insufficient for unambiguous identification.

Also, views arising from OH-PLIF imaging of MILD combustion differ and seem to suggest that OH may not be a reliable marker for HRR. For example, OH-PLIF imaging of MILD combustion in a jet-in-hot-coflow (JHC) or a furnace showed thin regions of OH with a clear peak and strong gradients (Medwell *et al.*, 2007; Duwig *et al.*, 2012; Plessing *et al.*, 1998; Ozdemir & Peters, 2001; Dally *et al.*, 2004). On the other hand, Medwell *et al.* (2009) observed that there is a decrease in OH concentration with an increase in $\mathrm{CH_2O}$ in MILD reaction zones compared to the conventional combustion. This raises some questions on the use of OH as a HRR marker for MILD combustion. Moreover, the regions captured in OH-PLIF may or may not correspond to heat releasing regions in MILD combustion because the unreacted mixture also contains OH. Indeed, some discrepancies were observed between $\mathrm{OH^*}$ and OH in another study (Sidey *et al.*, 2014) suggesting that OH may not necessarily coincide with primary heat release under MILD conditions. However, the $\mathrm{OH^*}$ chemiluminescent signal is known to correspond well to HRR zones and their gross features but it is inadequate to capture the fine features of these zones required for model development.

Past DNS studies investigated the adequacy of commonly used HRR chemical markers and suggested that two-scalar markers such as $(\mathrm{OH} \times \mathrm{CH_2O})$ or $(\mathrm{H} \times \mathrm{CH_2O})$ rather than a single scalar were good in identifying HRR regions in MILD combustion (Nikolaou

& Swaminathan, 2014; Minamoto & Swaminathan, 2014; Chi *et al.*, 2018; Wabel *et al.*, 2018). However, these studies are for premixed combustion under either conventional or MILD conditions. Here, our interest is to extend those assessments of HRR markers for MILD combustion with mixture fraction variation using DNS data of Doan *et al.* (2018). This specific interest is because the inception of MILD combustion does not follow the classical routes due to the chemical kinetic role of radicals present in the unreacted mixture as has been shown by Doan & Swaminathan (2019). Also, the presence of both premixed and non-premixed modes in MILD combustion with mixture fraction variation was shown by Doan *et al.* (2018) using the Flame Index (FI) analysis (Yamashita *et al.*, 1996; Briones *et al.*, 2006). Recently, Hartl *et al.* (2018) suggested that the CEMA (chemical explosive mode) analysis of Lu *et al.* (2010) can be used to distinguish premixed from non-premixed regions in partially premixed combustion. Hence, a comparative analysis using the above two, FI & CEMA, techniques is of interest here. Furthermore, MILD combustion is expected to give nearly homogeneous temperature and density fields and thus, the schlieren imaging could be used to distinguish combustion under conventional and MILD conditions. This will also be explored here.

This paper is organised as follows. The methodology used to conduct the DNS is briefly presented in Section 2. Sections 3.1 and 3.2 discuss, respectively, the adequacy of some heat release rate markers and the comparison between CEMA and flame index analyses to distinguish non-premixed from premixed combustion. The analysis using numerical schlieren is investigated in Section 3.3. A summary of the main findings is provided in the final section.

2 DNS of MILD combustion

The DNS data of Doan *et al.* (2018) are of non-premixed MILD combustion of methane-air mixture diluted with recirculated exhaust gases at atmospheric pressure inside a cube

of size $L_x \times L_y \times L_z = 10 \times 10 \times 10$ mm^3. The procedures used to conduct the DNS are illustrated in Fig. 1. Details of these procedures are described by Doan *et al.* (2018) and a brief summary is provided below for the sake of completeness. The initial and inflowing fields of mixture fraction, Z, reaction progress variable, c, scalar mass fractions, Y_α, and velocity fields, u_i, were generated in 5 preprocessing steps, marked as steps 1 to 5 in Fig. 1.

The required turbulence field was obtained in step 1 by simulating a decaying homogeneous isotropic turbulence. Laminar premixed flames under MILD conditions with a reactant temperature of $T_r = 1500$ K were computed for various Z values and the scalar mass fractions are tabulated as a function of Z and c in step 2. An initial turbulent mixture fraction, $\widehat{Z}$, and reaction progress variable, $\widehat{c}$, were constructed with prescribed means, $\langle Z \rangle$ and $\langle c \rangle$, and length scales ℓ_Z and ℓ_c in step 3. The symbol $\langle \cdot \rangle$ means quantities averaged over the entire computational volume. The mixture fraction definition of Bilger *et al.* (1990) was used for Z and the reaction progress variable was based on fuel mass fraction. The species mass fractions $Y_\alpha(c, Z)$ obtained in step 2 were mapped onto $\widehat{Z}$ and $\widehat{c}$ fields in step 4. The turbulence from step 1 and scalar fields from step 4 were then allowed to interact in step 5 for about 40 μs, which is approximately one large eddy turnover time of the initial turbulence field of step 1. This time is much shorter than the lowest reference ignition delay time, which is about 5 ms, for the methane-air mixture conditions considered for this study but long enough to ensure that the scalar and turbulent flow fields have interacted sufficiently before the combustion begins. This ignition delay time was computed using a PSR configuration with fuel-air mixtures diluted with only CO_2, N_2, and H_2O without radical species as normally done for reference ignition delay time calculation. However, there are radical species present in the mixture and thus the actual delay time can be shorter than the reference value of 5 ms. If one uses the volume-averaged values of the various species from the step 4 for the PSR calculation then the c_T value increases by about 10% over a time of 140 μs. This time is sufficiently

larger than the mixing time of 40 μs used in the step 5. Also, this delay time is shorter than the residence time.

One could also use other canonical configurations such as a PSR or a counterflow flame instead of a freely propagating premixed flame for step 2 of the preprocessing stage described above to obtain the various scalar fields as a function of Z and c. However, it has been shown by Doan (2018) that $Y_\alpha(c, Z)$ does not vary unduly for these configurations.

The scalar fields obtained at the end of step 5 included unburnt ($c = 0$), burnt ($c = 1$) and partially burnt (intermediate values of c) mixtures with equivalence ratio, $\widehat{\phi} = \widehat{Z}\left(1-\widehat{Z}_{st}\right) / \left(\widehat{Z}_{st}\left(1-\widehat{Z}\right)\right)$, where Z_{st} is the stoichiometric mixture fraction, varying from 0 to 10 inside the computational domain. These preprocessed fields were then used as the initial and inflowing conditions for the MILD combustion DNS in the second stage as shown in Fig. 1. Further details can be found in Doan *et al.* (2018).

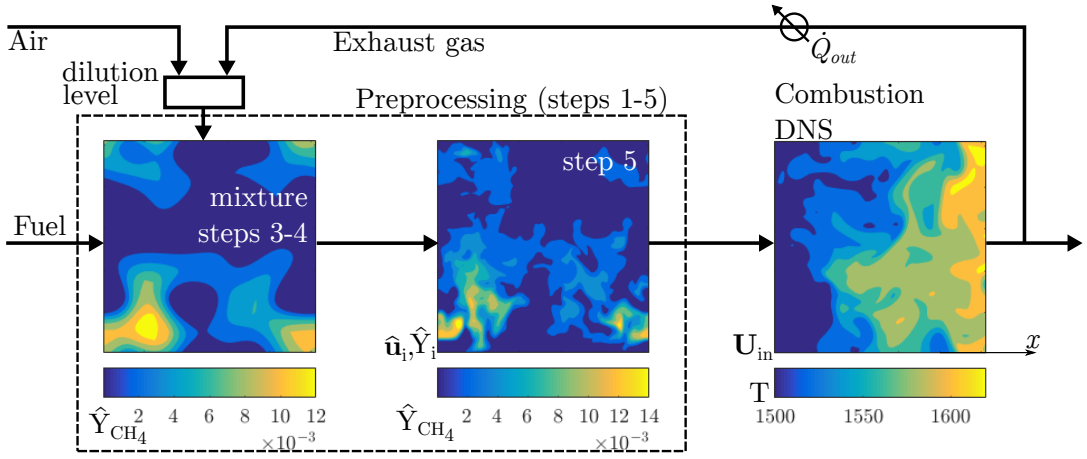

Figure 1. Schematic illustration of the DNS steps followed for the non-premixed MILD combustion of methane and air diluted with recirculated exhaust gases (from Doan *et al.* (2018)).

Three cases were simulated by Doan *et al.* (2018) and their details are given in Tables 1 and 2. The first two cases, AZ1 and AZ2, used the same oxidiser with 3.5% O_2 (by volume) but differed in the length scale ratio, ℓ_c/ℓ_Z. The third case BZ1 had more diluted oxidiser (2% of O_2) and the same length scale ratio as AZ1, see Table 1. The case of $\ell_c/\ell_Z > 1$ was not considered because the mixture fraction mixing length scales are

generally larger than the chemical length scales such as the flame thickness or ignition kernel size at T_r as large as 1500 K. All cases had a similar turbulence field with an integral length scale of $\Lambda_0 \approx 1.42$ mm and root-mean square value of $u' \approx 16.66$ m/s for the velocity fluctuations. This yielded turbulence and Taylor microscale Reynolds numbers of $\mathrm{Re}_t \approx 96$ and $\mathrm{Re}_\lambda \approx 34.73$ respectively.

Table 1. Oxidiser composition for the initial MILD mixture.

Case	$X_{\mathrm{O}_2,ox}$	$X_{\mathrm{H}_2\mathrm{O},ox}$	$X_{\mathrm{CO}_2,ox}$	$X_{\mathrm{N}_2,ox}$
AZ1-2	0.035	0.134	0.067	0.764
BZ1	0.020	0.46	0.073	0.761

Table 2. MILD combustion DNS initial conditions.

Case	Λ_0/ℓ_Z	$\langle X_{\mathrm{O}_2}\rangle$	$X_{\mathrm{O}_2}^{\max}$	ℓ_c/ℓ_Z	$\langle Z\rangle$	Z_{st}	σ_Z^2	$\langle c\rangle$	σ_c^2
AZ1	0.60	0.0270	0.035	0.77	0.008	0.010	0.00007	0.56	0.068
AZ2	0.79	0.0285	0.035	0.99	0.008	0.010	0.00011	0.56	0.078
BZ1	0.60	0.0160	0.020	0.77	0.0046	0.0058	0.00003	0.56	0.068

The numerical domain was specified to have inflow and non-reflecting outflow boundary conditions in the x-direction and periodic conditions in the transverse, y and z, directions. The numerical domain was discretised using uniformly distributed $512 \times 512 \times 512$ grid points to ensure that all chemical and turbulence length scales were resolved (Doan *et al.*, 2018). A combination of Smooke & Giovangigli (1991) and Bilger *et al.* (1990) mechanisms for methane-air combustion was used for the combustion kinetics along with OH^* chemistry from Kathrotia *et al.* (2012). The resulting mechanism involved 19 species and 58 reactions, and balanced the accuracy and computational cost appropriately by giving a good agreement for the measured values of the laminar flame speeds and ignition delay times. Details and validation of this mechanism are discussed by Doan *et al.* (2018).

The numerical code SENGA2 was used to solve the fully compressible conservation equations for mass, momentum, internal energy and species mass fractions, Y_α. A tenth order central difference scheme was used for spatial discretisation and a third order low storage Runge-Kutta scheme for time integration. The transport and thermo-chemical

properties were temperature dependent with non-unity constant Lewis numbers. Each case was run for $1.5\tau_f$, where the flow-through time is $\tau_f = L_x/U_{in}$ with $U_{in} = 20\mathrm{m/s}$ as the inflowing velocity. The simulations used a timestep of $\delta t = 1$ ns. Samples, about 50 snapshots for statistical analysis, were taken after the first flow-through time to ensure that the initial transients had left the domain. These simulations have been run on ARCHER, a Cray XC30 system, and each simulation took approximately 550 wall-clock hours using 4096 cores.

In addition to the MILD combustion cases listed in Table 2, two turbulent premixed and a premixed MILD combustion cases are also used for comparative analysis using numerical schlieren to be discussed in Section 3.3. The characteristics of these three cases are summarised in Table 3. The premixed MILD combustion case of Minamoto & Swaminathan (2014), case P3 in Table 3, was simulated using the method described above and keeping the equivalence ratio of $\phi = 0.8$ to be constant across the whole domain with a reactant temperature of 1500 K. The oxidiser stream had the same composition as the one used for the cases AZ1 and AZ2 detailed in Table 1. The other premixed cases are statistically planar flames propagating in a rectangular domain with boundary conditions similar to that used for the MILD cases described above. The case P2 considered a stoichiometric flame with a one-step chemistry mechanism while case P1 is for conventional methane/air combustion with an equivalence ratio of 0.8 with reactants temperature of 600 K. The Damköhler and Karlovitz numbers are respectively defined as $Da = \Lambda_0 s_L/(\delta_{th} u')$ and $Ka = (u'/s_L)^{3/2}(\delta_{th}/\Lambda_0)^{1/2}$, where the laminar flame speed and its thermal thickness are s_L and δ_{th} respectively. Detailed descriptions of these cases can be found in the references cited in Table 3.

Table 3. Conditions of additional DNS data used for numerical schlieren analysis.

Case	u'/s_L	ϕ	Λ_0/δ_{th}	Re_t	Da	Ka	Ref.
P1	2.19	0.8	2.11	38.5	0.97	2.22	Case C of Minamoto & Swaminathan (2014)
P2	11.25	1.0	3.75	110.0	0.33	19.5	Case K of Gao *et al.* (2014)
P3	9.88	0.8	1.15	96.1	0.69	11.9	Case B of Minamoto & Swaminathan (2014)

3 Results and discussion

Figure 2 shows the volume rendered temperature field for a conventional premixed combustion case, P1, and the MILD combustion, case AZ1. These figures can be related to digital photographs from experiments showing the variation in luminescence of a flame. The existence of a flame front, and thus strong temperature gradient, in the conventional premixed combustion case is observed. On the other hand, a homogeneous temperature field is observed for the MILD case, which is similar to those observed in photographs from MILD combustion experiments (de Joannon *et al.*, 2000). The volumetrically distributed reaction zones and their frequent interactions result in homogeneous and mild temperature rise resulting in the homogeneous field seen in Fig. 2b. This behaviour was observed for both premixed (Minamoto *et al.*, 2014*b*) and non-premixed MILD combustion (Doan *et al.*, 2018). For the premixed case P2, the behaviour is similar to the P1 case but with increased wrinkling because of higher turbulence level.

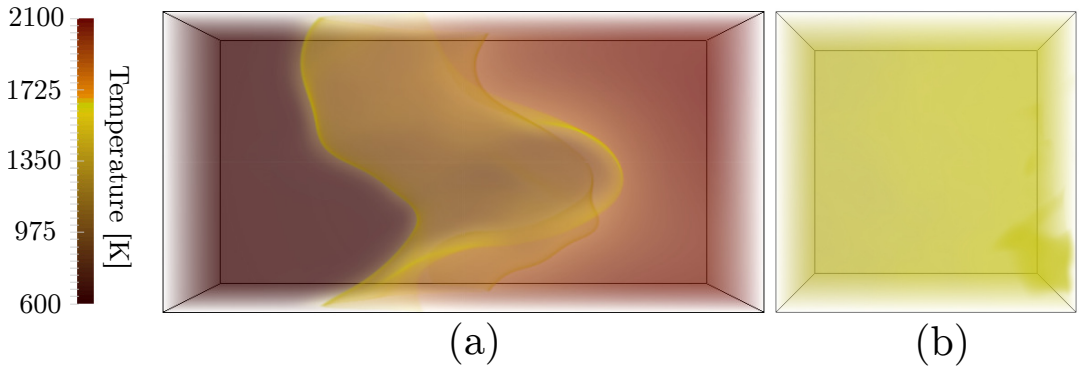

Figure 2. Volume rendered temperature field of (a) conventional turbulent premixed combustion, Case P1, and (b) MILD combustion of Case AZ1.

It is quite common to use OH in experimental studies of turbulent combustion to deduce information on the distribution of heat release rate in general and this approach has also been used for MILD combustion in past studies. This radical is formed in the flame but it does not go to zero in hot products. Thus, it may become hard to distinguish the OH formed in heat releasing regions from those in the recirculated hot products for

MILD combustion. Furthermore, the level of OH formed in the reaction zones may be comparable to or smaller than the background OH level in MILD combustion. These scenarios are assessed carefully in the following discussion. Figure 3 shows the contours of heat release rate, Y_{OH} and ΔY_{OH} for case AZ1. The typical results are shown for the mid x-y plane at $t = \tau_f$. The heat release rate is concentrated in thin regions even in non-premixed MILD combustion as has been observed by Minamoto & Swaminathan (2014) for premixed MILD combustion. Also, the heat release or chemical reactions start to occur from the inlet plane because of the radicals present in the incoming mixture as observed in earlier MILD combustion studies. This is physical and one would expect this if a computational boundary cuts through reacting regions.

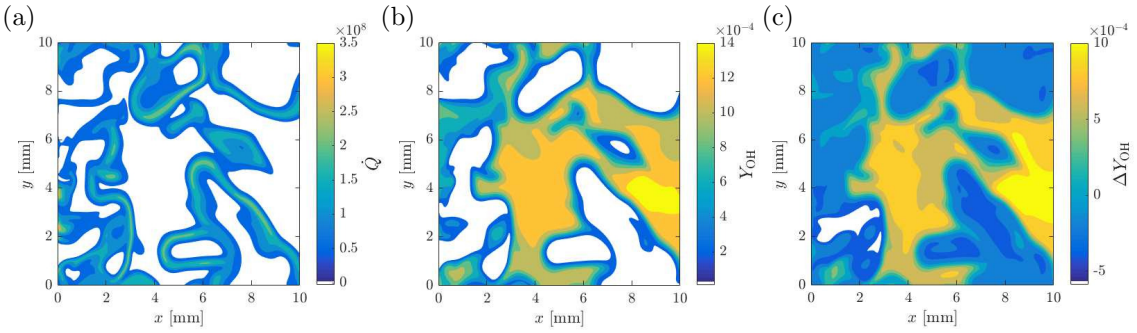

Figure 3. Contours of (a) heat release rate, (b) Y_{OH} and (c) ΔY_{OH} in the mid x-y plane at $t = \tau_f$ in case AZ1.

The corresponding spatial variation of OH mass fraction is shown in Fig. 3b. The large values of Y_{OH} are seen in regions of negligible heat release rate and these regions contain burnt gases. This is verified by analysing the relative mass fractions of H_2O, CO_2, etc, which are not shown here. The negligible heat release in these regions can be easily verified by comparing Figs. 3a and 3b. However, if one traces the locations of large $|\nabla Y_{\mathrm{OH}}|$ then it is quite easy to see that this locus (not shown) follows along the large heat release rate depicted in Fig. 3a and the values of Y_{OH} along this locus are nearly 20 to 30% of its peak value. The LIF imaging of such situation is likely to capture the product gas regions (large OH values) quite vividly and mask the heat releasing locations.

Furthermore, these smaller values may not be substantially larger than the background OH levels coming from the recirculated exhaust gases. This is verified in Fig. 3c by showing the variation of $\Delta Y_{\mathrm{OH}} = Y_{\mathrm{OH}}^{\mathrm{R}} - Y_{\mathrm{OH}}^{\mathrm{CD}}$. The mass fraction of OH shown in Fig. 3b is denoted by $Y_{\mathrm{OH}}^{\mathrm{R}}$, and $Y_{\mathrm{OH}}^{\mathrm{CD}}$ represents the local OH mass fraction value arising from the recirculated hot gases entering through the inlet plane. The latter value is obtained by re-running the case AZ1 but with no reaction and thus there are only convective and diffusive processes. Alternatively, one can conduct another reacting DNS with a passive scalar to represent the incoming OH to obtain $Y_{\mathrm{OH}}^{\mathrm{CD}}$. Here, we took the former approach because (i) the reacting DNS was conducted for an earlier study and repeating it is very expensive because of the stiff chemical reactions and (ii) more importantly, the changes in the local velocity between the reactive and non-reactive (convective-diffusive) cases are observed to be very small because the temperature rise from the heat release rate is only about 150 K. Hence, this approach cannot be used for the conventional combustion cases.

A positive value of ΔY_{OH} implies that the combustion produced OH is larger than the background value. The negative value implies that (i) the local value is the background value coming from the convective-diffusive processes in regions with no heat release rate or (ii) $Y_{\mathrm{OH}}^{\mathrm{CD}}$ is larger than $Y_{\mathrm{OH}}^{\mathrm{R}}$ in regions with non-negligible heat release. The second case seems to be paradoxical but it is physical - MILD combustion starts in regions with $\Delta Y_{\mathrm{OH}} < 0$ as has been shown by Doan & Swaminathan (2019) and the production of OH in these regions is smaller than the consumption of the background OH. The values of ΔY_{OH} is around zero in the locations corresponding to the large heat release rate (cf. Figs. 3a and 3c). Thus, one needs to be cautious while interpreting OH-PLIF images to deduce characteristics of reaction zones or to identify heat releasing regions in MILD combustion.

The pdf (probability density function) of ΔY_{OH} constructed from the DNS data is shown in Fig. 4 for the case AZ1. This pdf conditioned on the heat release rate, $\dot{Q}$, shows that the most probable value of ΔY_{OH} is about 1×10^{-4} which is nearly 1/10th of the

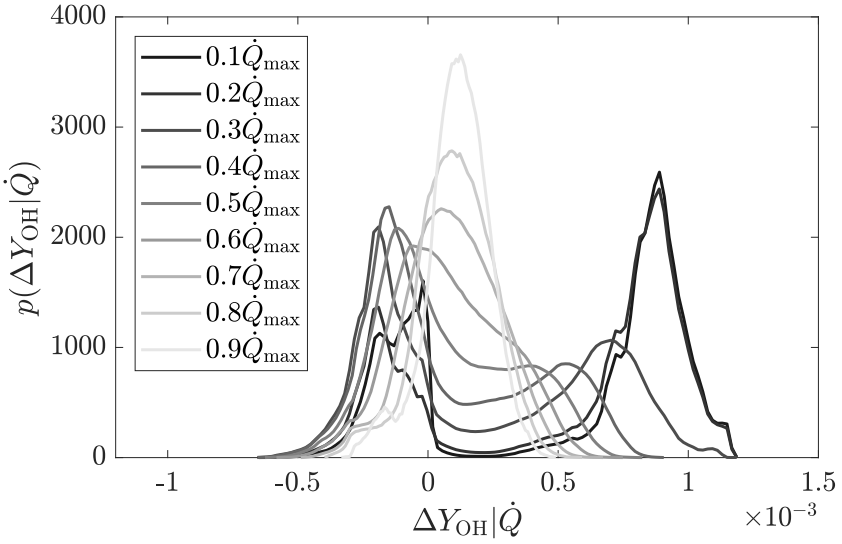

Figure 4. Pdf of $\Delta Y_{\mathrm{OH}} = Y_{\mathrm{OH}}^{\mathrm{R}} - Y_{\mathrm{OH}}^{\mathrm{CD}}$ from Case AZ1 at $t = \tau_f$.

most probable largest value observed in the low heat releasing regions. The right peak for the low heat release rate corresponds to the burnt mixtures while the left peak is for the mixtures beginning to react. This behaviour would be similar for the more diluted case BZ1 (not shown). These results point out that LIF imaging for MILD combustion needs more care and closer attention. The commonly employed LIF markers for the heat release are investigated next.

3.1 Markers for Heat Release

The chemical markers for heat release used in experiments are based on chemiluminescence or LIF of some species. One can deduce the LIF signals using the DNS data and thus it is possible to evaluate the adequacy of these methods by comparing the heat release from the DNS to those obtained using the deduced LIF signals. This has been done in many past studies for premixed combustion (Nikolaou & Swaminathan, 2014; Minamoto & Swaminathan, 2014; Chi *et al.*, 2018; Wabel *et al.*, 2018) and also for premixed MILD combustion (Minamoto & Swaminathan, 2014). However, it is not quite easy to deduce the chemiluminescence signal from DNS unless the chemiluminescent species are trans-

ported in the simulations. The current DNS of non-premixed MILD combustion included OH^*, one of the chemiluminescence species, in the chemical kinetic mechanism and thus this transported OH^* can be used.

The PLIF signal, S_α, of a species α depends on the species molar concentration $[\alpha]$ and temperature. This dependence is given by

$$S_\alpha \propto [\alpha]\, T^{(1-\beta)}. \tag{1}$$

The commonly used species for PLIF are $\mathrm{CH_2O}$, OH, and HCO. The LIF of atomic hydrogen H needs two-photon techniques as has been demonstrated in past studies (Kulatilaka *et al.*, 2009; Mulla *et al.*, 2016; Marshall & Pitz, 2018) and is also analysed here. The values of β for this study is set to be 2.6 for $\mathrm{CH_2O}$, 0 for OH and 1.25 for HCO based on past experimental studies (Najm *et al.*, 1998; Paul & Najm, 1998). The value of this parameter for the atomic hydrogen is 2 (Kulatilaka *et al.*, 2009). There are, however, some uncertainties for the β values but the results did not change unduly if slightly different values are used. As noted in the Introduction, the product of two LIF signals, for example $(\mathrm{OH} \times \mathrm{CH_2O})$ or $(\mathrm{H} \times \mathrm{CH_2O})$, is also used to mark heat releasing regions in combustion of hydrocarbon-air mixtures. Hence, we shall consider these two-scalar based markers also.

Figure 5 compares the synthesised PLIF signals for various heat release markers. These typical results, extracted using a single snapshot, are shown in the mid x-y plane for the case AZ1. All of the quantities shown in the figure are normalised using their respective maximum values in the mid x-y plane and these normalised quantities are denoted using a 'tilde'. It is observed that the synthesised single species markers of OH, $\mathrm{CH_2O}$ and H do not represent the features of heat release shown in Fig. 5a quite well. Indeed, Figs. 5b and 5d depicting the OH- and H-PLIF signals show that these two species are present in the downstream regions with nearly no reaction and they do not show up in heat

releasing regions in the upstream part. This is because OH and H radicals are consumed in the upstream regions where MILD combustion begins (Doan & Swaminathan, 2019). As one moves downstream, these species are found in regions with small heat release as products of combustion. On the other hand, the precursor species CH_2O is present in some of the upstream non-reacting regions. Only $\widetilde{S_{\mathrm{HCO}}}$ shown in Fig. 5e represents the $\widetilde{\dot{Q}}$ well. The two-scalar based markers $S_{\mathrm{OH}} \widetilde{\times S_{\mathrm{CH_2O}}}$ and $S_{\mathrm{H}} \widetilde{\times S_{\mathrm{CH_2O}}}$ also reproduce most features of the heat releasing zones quite well. The PLIF image of $S_{\mathrm{H}} \widetilde{\times S_{\mathrm{CH_2O}}}$ is similar to $S_{\mathrm{OH}} \widetilde{\times S_{\mathrm{CH_2O}}}$ and so it is not shown here.

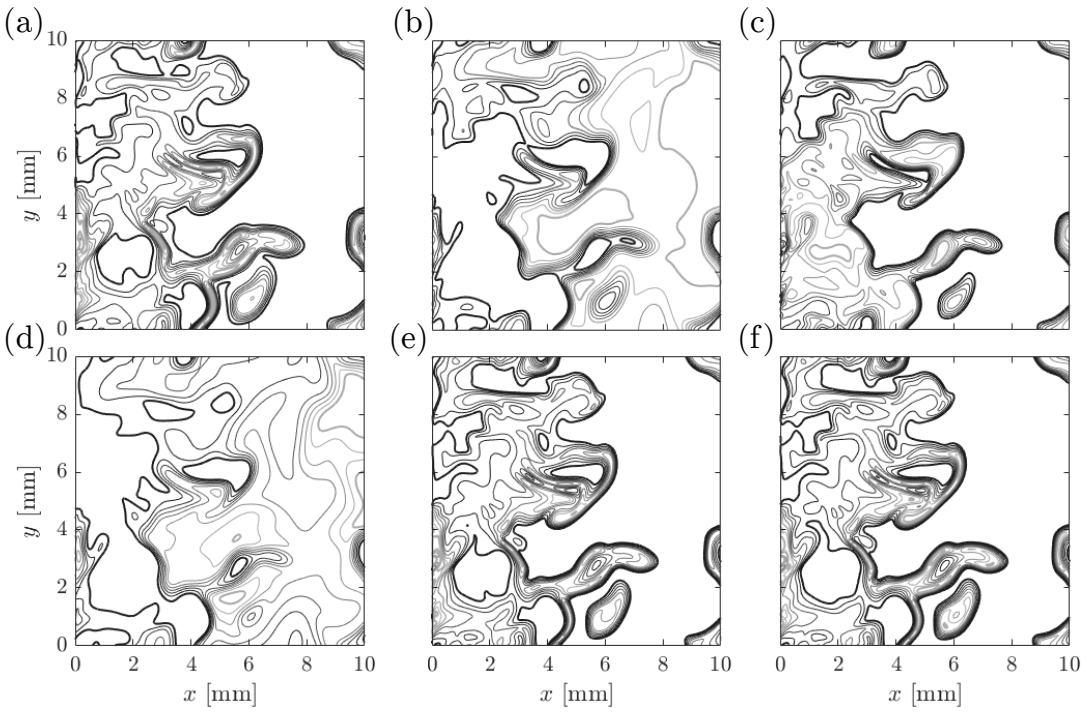

Figure 5. Contours of (a) $\widetilde{\dot{Q}}$, (b) $\widetilde{S_{\mathrm{OH}}}$, (c) $\widetilde{S_{\mathrm{CH_2O}}}$, (d) $\widetilde{S_{\mathrm{H}}}$, (e) $\widetilde{S_{\mathrm{HCO}}}$ and (f) $S_{\mathrm{OH}} \widetilde{\times S_{\mathrm{CH_2O}}}$ in the mid x-y plane for case AZ1 at $t = 1.5\tau_f$. Dark to light gray lines are for iso-contours of values 0.1, 0.2, ..., 0.9.

The spatial correlation seen in Fig. 5 becomes clearer if one cross plots the LIF signal with the heat release rate since a good marker should have the data points along the diagonal. Figure 6 shows the scatter plot for the case shown in Fig. 5. These results do not change unduly if one uses the data from various planes or the entire computational volume or at different time instants. It is clear that the PLIF of OH, H and CH_2O are

inadequate. As discussed earlier, $\widetilde{S_{\mathrm{OH}}}$ shows a large scatter since it is present in regions of low heat release and it is absent in the upstream heat releasing regions. Although $\widetilde{S_{\mathrm{CH2O}}}$ is similar to that for $\widetilde{S_{\mathrm{OH}}}$, it behaves differently. It is overly present in the upstream regions just ahead of heat releasing regions and absent in downstream regions as one would expect for a precursor. This is consistent with the findings of Medwell *et al.* (2009) where both OH and CH_2O were exhibiting different behaviours than in the conventional combustion, which led to *reaction weakening* in MILD combustion. The atomic hydrogen H behaves somewhat similar to OH (see Figs. 5b and 5d also). Figures 6e and 6f depict that the $\widetilde{S_{\mathrm{HCO}}}$ and the two-scalar marker $\left(S_{\mathrm{OH}} \widetilde{\times S_{\mathrm{CH_2O}}}\right)$ are good. The marker $\left(S_{\mathrm{H}} \widetilde{\times S_{\mathrm{CH_2O}}}\right)$ behaves very similar to $\left(S_{\mathrm{OH}} \widetilde{\times S_{\mathrm{CH_2O}}}\right)$ and thus it is not shown here. The result of $\widetilde{[\mathrm{OH}^*]}$ will be discussed later.

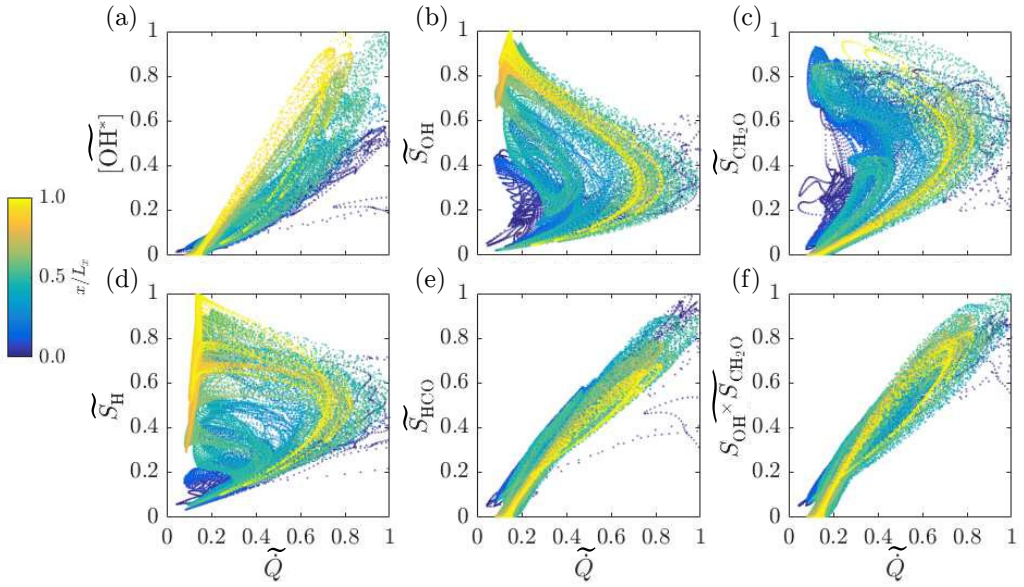

Figure 6. Scatter plots of normalised heat release rate vs (a) $\widetilde{[\mathrm{OH}^*]}$, (b) $\widetilde{S_{\mathrm{OH}}}$, (c) $\widetilde{S_{\mathrm{CH_2O}}}$, (d) $\widetilde{S_{\mathrm{H}}}$, (e) $\widetilde{S_{\mathrm{HCO}}}$ and (f) $S_{\mathrm{OH}} \widetilde{\times S_{\mathrm{CH_2O}}}$ for case AZ1 obtained using the data shown in Fig. 5. Points are coloured by their streamwise locations.

The correlation between the various markers and heat release is quantified in Table 4 using the Pearson correlation coefficient. It is observed that $\widetilde{S_{\mathrm{HCO}}}$, $\left(S_{\mathrm{OH}} \widetilde{\times S_{\mathrm{CH_2O}}}\right)$ and $\left(S_{\mathrm{H}} \widetilde{\times S_{\mathrm{CH_2O}}}\right)$ are the only adequate HRR markers since their correlation coefficients

are generally larger than 0.9. Although the correlation coefficient for $\widetilde{S_{\mathrm{HCO}}}$ is about 0.95 it is generally hard to use this marker because of its low signal-to-noise ratio (Paul & Najm, 1998; Tanahashi *et al.*, 2005) but this has been improved recently using multimode lasers (Kiefer *et al.*, 2009; Zhou *et al.*, 2014). The coefficients for the other cases are also listed in Table 4. Although there is some variations among the cases, the relative merit of various markers noted above for the case AZ1 also holds for other cases. These correlation coefficients do not change if one uses data from another plane or the entire computational volume or multiple snapshots. This is because, the MILD combustion is homogeneous (see Fig. 2).

Table 4. Pearson correlation coefficients for the $\widetilde{\dot{Q}}$-$\widetilde{S_\alpha}$ scatter plots.

Case	$\widetilde{[\mathrm{OH}^*]}$	$\widetilde{S_{\mathrm{OH}}}$	$\widetilde{S_{\mathrm{CH_2O}}}$	$\widetilde{S_{\mathrm{H}}}$	$\widetilde{S_{\mathrm{HCO}}}$	$\widetilde{S_{\mathrm{OH}} \times S_{\mathrm{CH_2O}}}$	$\widetilde{S_{\mathrm{H}} \times S_{\mathrm{CH_2O}}}$
AZ1	0.9153	-0.4835	0.5407	-0.1454	0.9447	0.9543	0.9549
AZ2	0.9431	0.0134	0.0890	0.3532	0.9511	0.9557	0.9306
BZ1	0.9458	0.2023	0.1091	0.4009	0.9529	0.9555	0.9279

In addition to the PLIF images discussed above, OH^* chemiluminescence signal is also used to identify heat releasing regions. This technique is based on the line-of-sight method implying that the information captured through this signal is averaged along the line of sight. Typically, CH^* or OH^* is used for this method. In this work, only OH^* is considered as it is the only chemiluminescent species available in the chemical mechanism used for the DNS (Doan *et al.*, 2018). The chemiluminescent signal is constructed using Eq. 1 without the temperature dependence employing the transported mole fraction of OH^*. Figure 7 shows the volume rendered (line-of-sight) images of normalised heat release rate $\widetilde{\dot{Q}}$ and $\widetilde{[\mathrm{OH}^*]}$ for a qualitative comparison. A reasonably good qualitative agreement between the two images is seen and gross features and locations of the heat releasing regions are captured quite well. However, there are some minor differences. The scatter plot of these two quantities is shown in Fig. 6a with the corresponding correlation coefficients listed in Table 4. Although there is some scatter in Fig. 6a, the correlation

coefficient is larger than 0.9 suggesting that OH^* is a good marker to identify heat releasing zones. This is specifically so when compared to OH which has a significantly lower correlation coefficient.

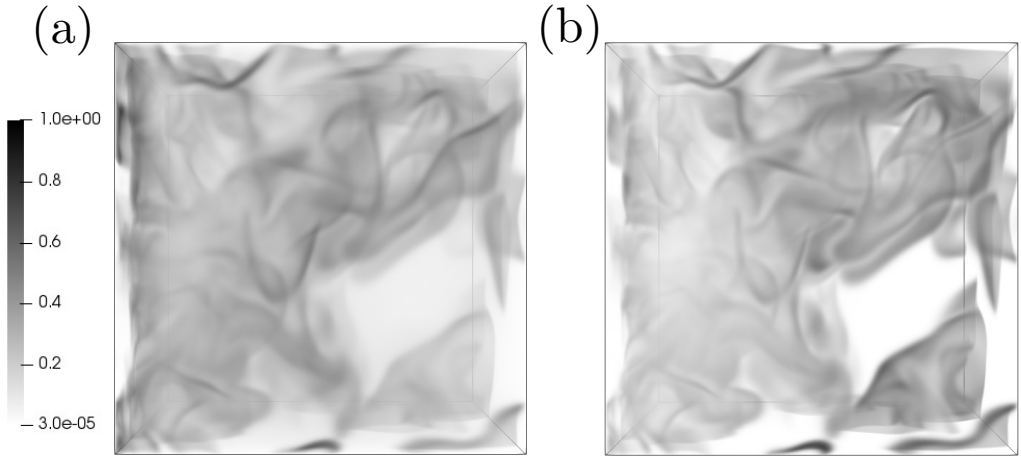

Figure 7. Volume rendered images of normalised (a) heat release rate, $\widetilde{\dot{Q}}$, and (b) $\widetilde{[\mathrm{OH}^*]}$ for the case AZ1.

3.2 Premixed or Non-premixed mode identification

Hartl *et al.* (2018) proposed a methodology to distinguish premixed from non-premixed modes in mixed-mode combustion using CEMA of Lu *et al.* (2010). The Jacobian of the chemical source term with respect to the thermodynamic quantities (temperature, species mole fractions and internal energy) is estimated first in this approach. Then, the eigenvalues of this Jacobian are computed and the eigenvalue with the largest real part, λ_e, is extracted. The CM indicator is obtained using this λ_e as

$$\mathrm{CM} = \text{sign}\left(\Re(\lambda_e)\right) \log_{10}\left(1 + |\Re(\lambda_e)|\right) \tag{2}$$

where $\Re(\lambda_e)$ is the real part of λ_e. A zero crossing of CM (sign changing from positive to negative) with a near constant mixture fraction value was noted to indicate premixed combustion. A region undergoing non-premixed combustion was characterised by the

presence of heat release and $\mathrm{CM} < 0$ with a large variation of mixture fraction. The temperature and major species measured using 1D Raman/Rayleigh measurements and minor species and reaction rates obtained from homogenous reactor calculations constrained by the measured quantities were used to calculate the CM indicator by Hartl *et al.* (2018). However, there is only one component of the local mixture fraction gradient in the 1D measurements along a line. Their study can be consulted for further details.

The DNS data can be used to compute the CM indicator directly and compared to the flame index, FI, analysis. The flame index originally proposed by Yamashita *et al.* (1996) was modified by Briones *et al.* (2006) to distinguish lean and rich premixed from non-premixed combustion. This FI is given by

$$\mathrm{FI} = \frac{Z - Z_{st}}{2|Z - Z_{st}|}\left(1 + \frac{\nabla Y_{\mathrm{CH_4}} \cdot \nabla Y_{\mathrm{O_2}}}{|\nabla Y_{\mathrm{CH_4}}||\nabla Y_{\mathrm{O_2}}|}\right) \tag{3}$$

where Z_{st} is the stoichiometric mixture fraction. The first part of the above equation is simply a "sign" or "signum" function. A zero value of FI indicates a non-premixed mode, while -1 and +1 respectively denote lean and rich premixed modes. The contribution of rich premixed combustion to the total heat release rate was shown to be smaller than 10% by Doan *et al.* (2018) for the non-premixed MILD combustion cases used for this study. This is because of the globally lean mixtures used for those DNS cases. The non-premixed mode contribution varied from 11% to 20% for the total heat release rate depending on the dilution level. Hence, the interest here is on the comparison of non-premixed combustion regions identified using the CM and FI indicators. Thus, regions with only $\mathrm{CM} < 0$ will be considered and these region should have $\mathrm{FI} = 0$. This analysis is done only for the non-premixed MILD cases, AZ1, AZ2 and BZ1, since they involve mixture fraction variations.

The variations of FI and CM for case AZ1 in the mid x-y plane are shown respectively in Figs. 8a and 8b. These are shown only for regions with the normalised heat release rate,

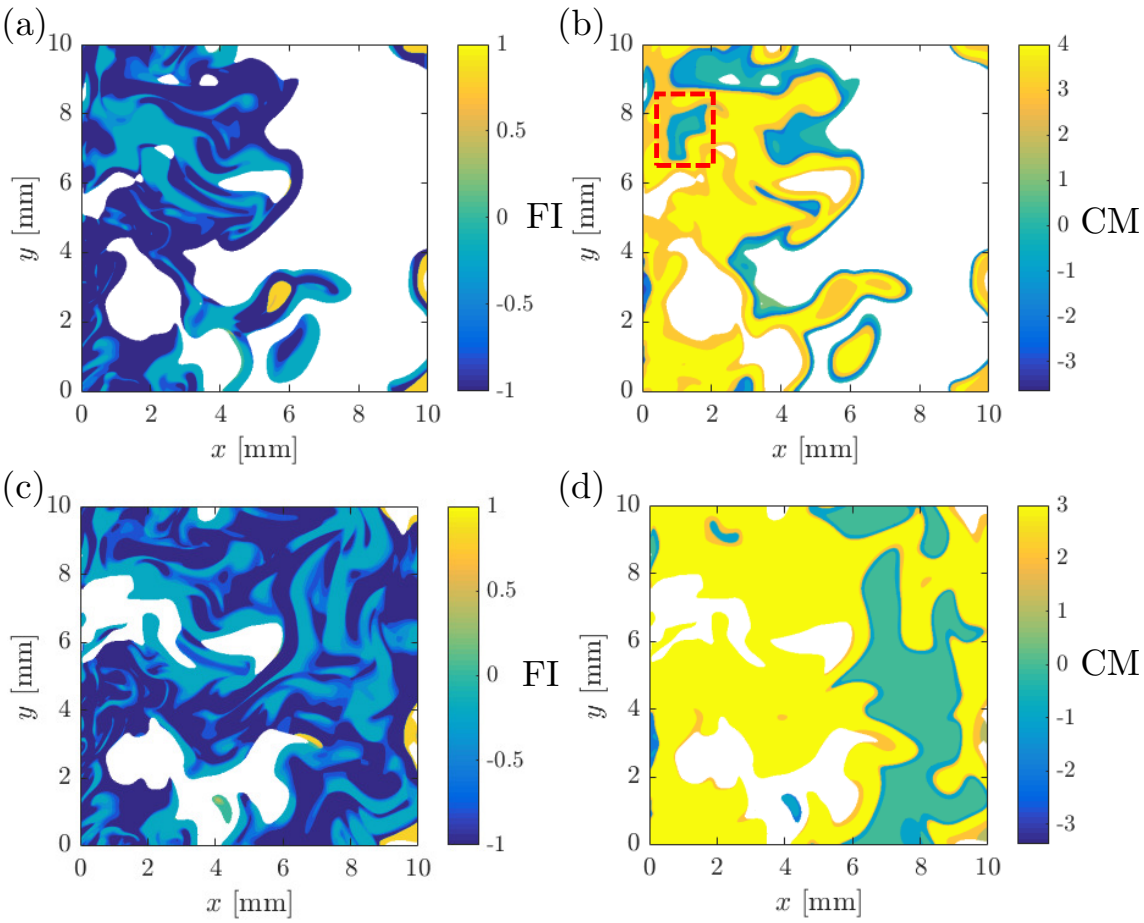

Figure 8. Variations of FI (in a,c) and CM (b,d) in the mid x-y plane for cases AZ1 (a,b) and BZ1 (c,d) at $t = 1.5\tau_f$. The results are shown for regions with $\dot{Q}^+ \geq 1.0$.

$\dot{Q}^+ = \dot{Q}\delta_{th}/(\rho_r s_L C_p(T_b - T_r))$, larger than 1 and the normalising quantities used are for the local mixture fraction value. The above conditioning on $\dot{Q}^+$ allows one to focus on regions with significant heat release where the FI and CM indices are meaningful. The results presented here are not unduly influenced by the exact value used for this threshold as long as sufficient number of regions (samples) with significant heat release rate are identified. The choice of $\dot{Q}^+ \geq 1$ is guided by earlier DNS studies of MILD combustion. It is observed that most of these regions have $\mathrm{CM} > 0$ indicating the presence of strong chemical activities or chemical explosive modes. There is, however, only a small region with $\mathrm{CM} < 0$ which is also marked in Fig. 8b. This region is supposed to be a non-premixed region which is also confirmed by the FI results, ie., $\mathrm{FI} = 0$, shown in Fig. 8a.

There are other regions with negative CM but these are indicated to be lean premixed regions by the FI.

The non-premixed mode contribution was shown to increase with increasing dilution by Doan *et al.* (2018) and thus it is instructive to see if this trend is captured by the CM indicator. The results for the case BZ1 are shown in Figs. 8c and 8d respectively for the FI and CM indicators. Indeed, there is an increase in the regions with $\mathrm{CM} < 0$ but these regions include those with lean premixed combustion (indicated by $\mathrm{FI} \simeq -1$). The qualitative comparisons shown in Fig. 8 suggest that there is some agreement between CM and FI indicators but there are large differences. The statistical behaviour of these quantities can be obtained by constructing the joint-pdf of FI and CM subject to the condition of $\mathrm{CM} < 0$ because of the interest here.

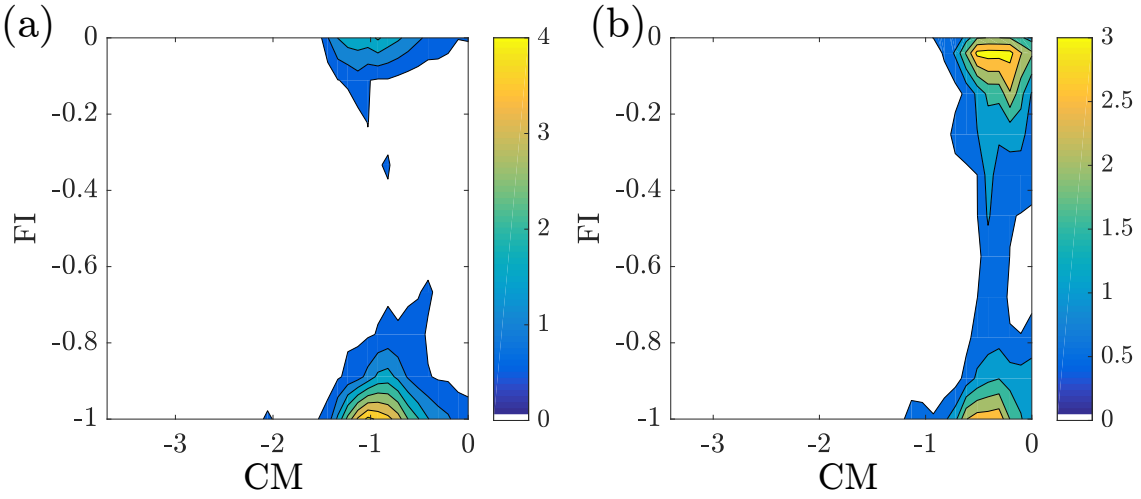

Figure 9. Joint-pdf of (CM, FI) in regions with $\dot{Q}^{+} \geq 1.0$ and $\mathrm{CM} < 0$ for cases (a) AZ1 and (b) BZ1 using samples collected in the mid x-y plane at $t = 1.5\tau_f$ shown in Fig. 8.

Figure 9 shows the joint-pdf of FI and CM subject to the condition $\mathrm{CM} < 0$ constructed using the samples collected from regions with $\dot{Q}^{+} \geq 1$ for both cases AZ1 and BZ1. The above two conditionings ensure that the identified reacting regions are non-premixed as per the views of Hartl *et al.* (2018). Thus, if the identified regions are indeed non-premixed then one would expect the joint-pdf contours to lie along $\mathrm{FI} = 0$ for all negative values of CM. The CM approach does capture some of the non-premixed regions

shown by the upper peak of the pdf and it also includes some lean premixed regions (lower peak). The second aspect comes from the inability to discriminate between a large patch of negative CM and the regions of negative CM around its zero crossings. The increased contribution of non-premixed mode with higher dilution is also seen in the joint-pdf for the case BZ1 shown in Fig. 9b, which is also captured by the CM marker. The joint-pdf constructed using samples, subject to the above two conditions, collected over the entire computational volume and the sampling period is similar to that shown in the figure above. Also, similar behaviour is observed for the case AZ2 and thus it is not shown here.

The above comparison showed that the approach using the CM indicator captures the existence of non-premixed mode to some extent. However, it focuses only on identifying regions of negative CM and does not distinguish the regions of negative CM associated with the zero crossing of CM (related to premixed combustion). Hence, the comparison did not distinguish lean premixed and non-premixed modes with CEMA while the FI approach did. Thus, further analysis is needed for this comparison using DNS and experimental data of turbulent partially premixed combustion under conventional and MILD conditions.

3.3 Schlieren approach

The next question that we like to tackle briefly is, how to appropriately discriminate the conventional from MILD combustion. This is quite hard to do using OH-LIF for the reasons discussed earlier. Indeed, direct photographs in furnace-like configuration showed no flame but some similarity with conventional flames were shown for MILD combustion in a JHC configuration as pointed out in the Introduction. Despite these, one of the main features reported for MILD combustion is the existence of mild gradients of temperature in experimental (Ozdemir & Peters, 2001; Wünning & Wünning, 1997) and DNS (Minamoto & Swaminathan, 2014) studies. The mild temperature gradient implies mild density gradient as well which is contrasting to a conventional flame having strong

density and temperature gradients. Thus, the schlieren method which employs density gradients can be the first step to assess whether the combustion is MILD or not.

A numerical schlieren image can be synthesised using the DNS data by computing (Hadjadj & Kudryavtsev, 2005):

$$Sc = \beta \, \exp\left(\frac{-\kappa \, |\nabla \rho|}{|\nabla \rho|_{\max}}\right) \tag{4}$$

with $\beta = 0.8$ and $\kappa = 15$. These are standard values used for numerical schlieren images and it was observed that the results discussed here are not sensitive to these specific values. Figure 10 shows the schlieren images obtained for the premixed flames (P1 & P2), premixed MILD combustion (P3) and the three non-premixed MILD combustion cases (see Tables 2 and 3). The technique is a line of sight method and thus the images shown has Sc from Eq. (4) integrated along the axis (z) normal to the images shown. The values given above for β and κ are used for all the cases shown in this figure and all the images are generated using the same greyscale so that they can be compared directly. Darker regions mark stronger density gradients, which is the preheat zone in conventional premixed flames, and brighter regions imply almost uniform density field (unreacted and burnt mixtures in premixed flames). The density gradient is almost negligible in reaction zones and thus it will be hard to identify distinctly in the schlieren image. Also, this is a line of sight technique and thus finer details such as flame wrinkling, etc., cannot be gathered from the schlieren images. However, the premixed combustion in flamelets and other regimes such as thin reaction zones or distributed flamelets can be distinguished quite easily. For example, the darker regions of the schlieren image will be thicker for the thin reaction zones combustion regime because the preheat zone with large density gradients is thickened by the small scale turbulence. This feature is seen for the premixed case P2 shown in Fig. 10b compared to the case P1 in Fig. 10a. The thickening of the preheat zone in thin reaction zones combustion can be seen clearly if a 2D cut of the DNS

data is used to construct the numerical schlieren image and this is shown in Fig. 11. It is quite obvious that the reaction zones marked using the iso-line of normalised heat release rate are thin and they are at the back end of the flame.

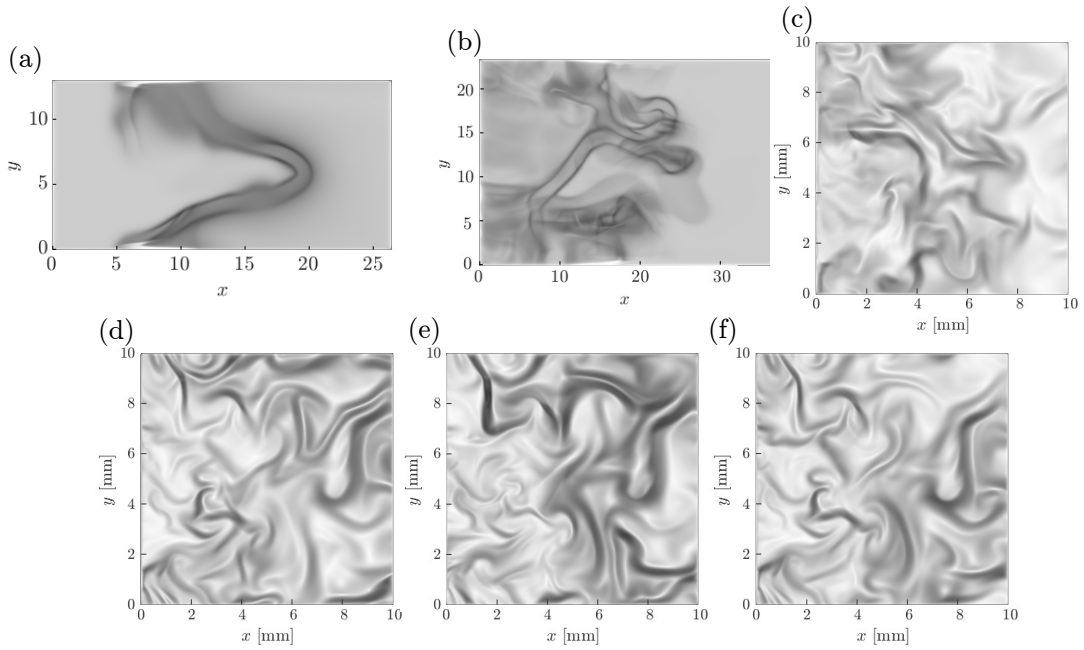

Figure 10. Numerical schlieren for the premixed cases (a) P1 and (b) P2, (c) premixed MILD combustion case P3 and the non-premixed MILD combustion cases (d) AZ1, (e) AZ2 and (f) BZ1. Axes for cases P1 and P2 are normalised by their respective laminar flame thicknesses.

The schlieren image for the premixed MILD combustion case is shown in Fig. 10c and for the non-premixed MILD combustion cases in Figs. 10d-f. These images are distinctly different from those for the premixed cases. The density gradients are distributed over a larger region and this gradient comes from flames, ignition fronts and mixing layers of hot products and cooler reactants. It is not straightforward to identify these three elements contributing to the density gradient. However, it is quite straightforward to distinguish MILD combustion from the conventional flames using the images such as those shown in Fig. 10. The mixing layers can be distinguished from the heat releasing regions by plotting iso-lines of normalised heat release rate in a representative plane as shown in Fig. 11a for the non-premixed MILD combustion case AZ1. The schlieren image shown

in this figure is also constructed using the density gradient in that representative plane. The darker regions with no heat release rate correspond to the mixing layers. These kinds of information is helpful to delineate MILD combustion from conventional flames. However, obtaining the kind of 2D information shown in Fig. 11 using schlieren in experimental studies may not be possible because the schlieren technique is a line of sight method and thus laser diagnostics are very much required to acquire finer information. Nevertheless, schlieren images help to quickly differentiate between MILD and conventional combustion and to establish that the conditions are indeed MILD before applying detailed laser diagnostics.

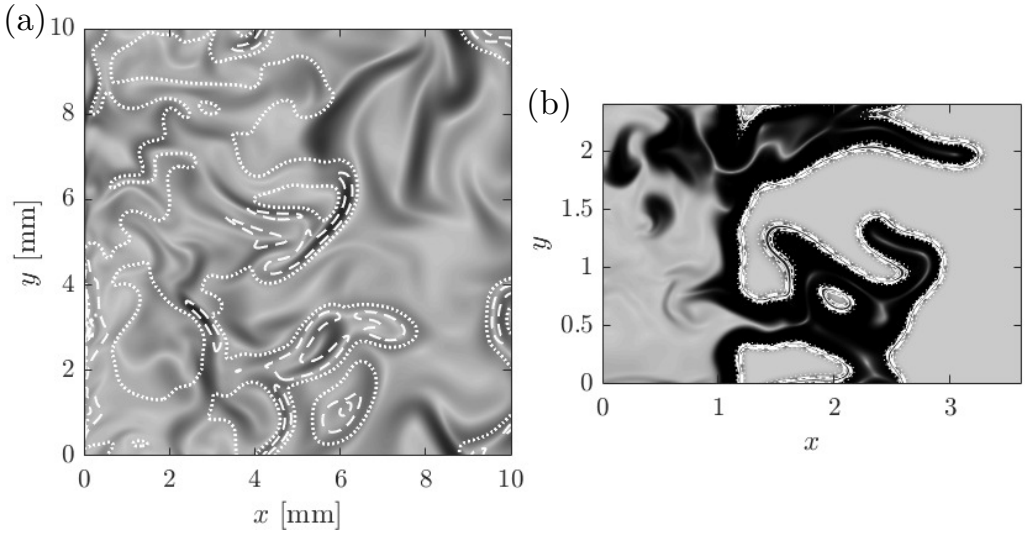

Figure 11. Numerical schlieren image for the data in the mid x-y plane of the (a) MILD combustion case AZ1 and (b) premixed combustion case P2. The iso-lines show the normalised heat release rate (white dotted line is for 0.2, dashed line is for 0.5, dash-dotted line is for 0.7 and solid line is for 0.9).

4 Conclusions

DNS data of turbulent premixed flames, premixed and non-premixed MILD combustion have been used to analyse the various markers employed to identify heat releasing, premixed and non-premixed reactions zones. For the heat release markers, several choices

used quite commonly in experimental studies of turbulent combustion were assessed for their suitability for MILD combustion by synthesising the laser induced fluorescence signals of these markers using the DNS data. Out of the various single-scalar heat release markers investigated, HCO was observed to be good but it has a poor signal-to-noise ratio which can be improved using multimode lasers (Kiefer *et al.*, 2009; Zhou *et al.*, 2014). The two-scalar markers $(\mathrm{OH} \times \mathrm{CH_2O})$ and $(\mathrm{H} \times \mathrm{CH_2O})$ were observed to identify the heat releasing zones well in combustion under both premixed and non-premixed MILD conditions. Since the recirculated hot gases in MILD combustion contain many of the single-scalar markers such as OH, one needs to be cautious in using them. The analysis of the DNS data showed that the local increase in the OH values above the background level is very small in regions of large heat release rate in MILD combustion and thus the commonly used OH-PLIF may not identify these regions of importance unambiguously. Hence, the heat releasing zone information deduced using OH-PLIF in MILD combustion must be used cautiously.

The chemiluminescent images based on OH^* obtained from the DNS data show a good correlation with heat releasing regions. However, these images are line-of-sight images and thus the finer information on the reaction zones such as their wrinkling, morphology and topology cannot be deduced. Nonetheless, the OH^* images allow for an improved identification of reaction zones compared to OH-PLIF for MILD combustion.

The non-premixed MILD combustion was shown to have premixed and non-premixed reaction zones along with autoignition (Doan *et al.*, 2018). Hartl *et al.* (2018) proposed a methodology using the CEMA concept to distinguish the premixed and non-premixed modes of combustion. This methodology is assessed along with the flame index (FI) using the DNS data. A comparison with the FI approach shows that the CEMA methodology identifies major parts of the non-premixed regions as premixed. Further work is required to delineate these regions and auto-ignition unambiguously.

The schlieren images deduced using the DNS data clearly identified the differences

between the conventional and MILD combustion qualitatively. The images from MILD combustion are characterised by mild gradients of temperature and density. Hence, schlieren imaging can be used to assess quickly whether a combustor is operating under MILD conditions or not before applying detailed laser diagnostics.

It should be noted that none of the methods discussed above helps to distinguish ignition from propagating flames since both are present in MILD combustion. Indeed, the interplay and importance of these two modes in MILD combustion were shown in past studies (Doan & Swaminathan, 2019; Minamoto *et al.*, 2014*a*) and thus, identifying a marker to distinguish them would allow for additional understanding of MILD combustion. Furthermore, some variations in the suitability of each marker for non-premixed MILD combustion is observed, depending on the dilution level, and analysing the causes behind these differences would also be of interest. This will be explored in future investigations.

Acknowledgements

N.A.K.D. acknowledges the financial support of the Qualcomm European Research Studentship Fund in Technology. This work used the ARCHER UK National Supercomputing Service (http://www.archer.ac.uk) using the computing time provided by EPSRC under the RAP project numbered e419 and the UKCTRF (e305).

References

BALACHANDRAN, R., AYOOLA, B.O., KAMINSKI, C.F., DOWLING, A.P. & MASTORAKOS, E. 2005 Experimental investigation of the nonlinear response of turbulent premixed flames to imposed inlet velocity oscillations. *Combust. Flame* **143** (1-2), 37–55.

BILGER, R. W., STARNER, S. H. & KEE, R. J. 1990 On Reduced Mechanisms for Methane-Air Combustion in Nonpremixed Flames. *Combust. Flame* **80**, 135–149.

BRIONES, A. M., AGGARWAL, S. K. & KATTA, V. R. 2006 A numerical investigation of flame liftoff, stabilization, and blowout. *Phys. Fluids* **18**, 043603.

CAVALIERE, A. & DE JOANNON, M. 2004 Mild Combustion. *Prog. Energy Combust. Sci.* **30** (4), 329–366.

CHI, C., JANIGA, G., ZÄHRINGER, K. & THÉVENIN, D. 2018 DNS study of the optimal heat release rate marker in premixed methane flames. *Proc. Combust. Inst.* p. (available online).

DALLY, B. B., RIESMEIER, E. & PETERS, N. 2004 Effect of fuel mixture on moderate and intense low oxygen dilution combustion. *Combust. Flame* **137** (4), 418–431.

DOAN, N. A. K. 2018 Physical Insights of Non-Premixed MILD Combustion using DNS. PhD thesis, University of Cambridge.

DOAN, N. A. K. & SWAMINATHAN, N. 2019 Role of radicals on MILD combustion inception. *Proc. Combust. Inst.* **37**, 4539–4546.

DOAN, N. A. K., SWAMINATHAN, N. & MINAMOTO, Y. 2018 DNS of MILD combustion with mixture fraction variations. *Combust. Flame* **189**, 173–189.

DUWIG, C., LI, B., LI, Z. S. & ALDÉN, M. 2012 High resolution imaging of flameless and distributed turbulent combustion. *Combust. Flame* **159** (1), 306–316.

FAYOUX, A., ZÄHRINGER, K., GICQUEL, O. & ROLON, J.C. 2005 Experimental and numerical determination of heat release in counterflow premixed laminar flames. *Proc. Combust. Inst.* **30** (1), 251–257.

GAO, Y., CHAKRABORTY, N. & SWAMINATHAN, N. 2014 Algebraic Closure of Scalar Dissipation Rate for Large Eddy Simulations of Turbulent Premixed Combustion. *Combust. Sci. Technol.* **186** (10-11), 1309–1337.

HADJADJ, A. & KUDRYAVTSEV, A. 2005 Computation and flow visualization in high-speed aerodynamics. *J. Turbul.* **6**.

HARTL, S., GEYER, D., DREIZLER, A., MAGNOTTI, G., BARLOW, R. S. & HASSE, C. 2018 Regime identification from Raman/Rayleigh line measurements in partially premixed flames. *Combust. Flame* **189**, 126–141.

DE JOANNON, M., SAPONARO, A. & CAVALIERE, A. 2000 Zero-dimensional analysis of diluted oxidation of methane in rich conditions. *Proc. Combust. Inst.* **28** (2), 1639–1646.

KATHROTIA, T., RIEDEL, U., SEIPEL, A., MOSHAMMER, K. & BROCKHINKE, A. 2012 Experimental and numerical study of chemiluminescent species in low-pressure flames. *Appl. Phys. B Lasers Opt.* **107** (3), 571–584.

KATSUKI, M. & HASEGAWA, T. 1998 The science and technology of combustion in highly preheated air. *27th Symp. Combust.* **27**, 3135–3146.

KIEFER, J., LI, Z.S., SEEGER, T., LEIPERTZ, A. & ALDÉN, M. 2009 Planar laser-induced fluorescence of HCO for instantaneous flame front imaging in hydrocarbon flames. *Proc. Combust. Inst.* **32** (1), 921–928.

KULATILAKA, W. D., FRANK, J. H. & SETTERSTEN, T. B. 2009 Interference-free two-photon LIF imaging of atomic hydrogen in flames using picosecond excitation. *Proc. Combust. Inst.* **32**, 955–962.

LI, Z.S., LI, B., SUN, Z.W., BAI, X.S. & ALDÉN, M. 2010 Turbulence and combustion interaction: High resolution local flame front structure visualization using simultane-

ous single-shot PLIF imaging of CH, OH, and CH2O in a piloted premixed jet flame. *Combust. Flame* **157** (6), 1087–1096.

LU, T. F., YOO, C. S., CHEN, J. H. & LAW, C. K. 2010 Three-dimensional direct numerical simulation of a turbulent lifted hydrogen jet flame in heated coflow: a chemical explosive mode analysis. *J. Fluid Mech.* **652**, 45–64.

MARSHALL, G. & PITZ, R. W. 2018 Evaluation of heat release indicators in lean premixed H2/air cellular tubular flames. *Proc. Combust. Inst.* **37**, in press, corrected proof.

MEDWELL, P. R., KALT, P. A. M. & DALLY, B. B. 2007 Simultaneous imaging of OH, formaldehyde, and temperature of turbulent nonpremixed jet flames in a heated and diluted coflow. *Combust. Flame* **148** (1-2), 48–61.

MEDWELL, P. R., KALT, P. A. M. & DALLY, B. B. 2009 Reaction Zone Weakening Effects under Hot and Diluted Oxidant Stream Conditions. *Combust. Sci. Technol.* **181** (7), 937–953.

MENON, S. 2018 Multi-scale subgrid modelling of turbulent premixed combustion at engine relevant conditions. *Combust. Sci. Technol.* **Special issue on UKCTRF Workshop 2018**.

MINAMOTO, Y. & SWAMINATHAN, N. 2014 Scalar gradient behaviour in MILD combustion. *Combust. Flame* **161** (4), 1063–1075.

MINAMOTO, Y., SWAMINATHAN, N., CANT, R. S. & LEUNG, T. 2014*a* Morphological and statistical features of reaction zones in MILD and premixed combustion. *Combust. Flame* **161** (11), 2801–2814.

MINAMOTO, Y., SWAMINATHAN, N., CANT, R. S. & LEUNG, T. 2014*b* Reaction Zones and Their Structure in MILD Combustion. *Combust. Sci. Technol.* **186** (8), 1075–1096.

MULLA, I. A., DOWLUT, A., HUSSAIN, T., NIKOLAOU, Z. M., CHAKRAVARTHY, S. R., SWAMINATHAN, N. & BALACHANDRAN, R. 2016 Heat release rate estimation in laminar premixed flames using laser-induced fluorescence of CH2O and H-atom. *Combust. Flame* **165**, 373–383.

NAJM, H. N., PAUL, P. H., MUELLER, C. J. & WYCKOFF, P. S. 1998 On the Adequacy of Certain Experimental Observables as Measurements of Flame Burning Rate. *Combust. Flame* **113** (3), 312–332.

NGUYEN, Q.-V. & PAUL, P. H. 1996 The time evolution of a vortex-flame interaction observed via planar imaging of CH and OH. *26th Symp. Combust.* **26** (1), 357–364.

NIKOLAOU, Z. M. & SWAMINATHAN, N. 2014 Heat release rate markers for premixed combustion. *Combust. Flame* **161** (12), 3073–3084.

OZDEMIR, I. B. & PETERS, N. 2001 Characteristics of the reaction zone in a combustor operating at mild combustion. *Exp. Fluids* **30** (6), 683–695.

PAUL, P. H. & NAJM, H. N. 1998 Planar laser-induced fluorescence imaging of flame heat release rate. *27th Symp. Combust.* **27** (1), 43–50.

PLESSING, T., PETERS, N. & WÜNNING, J. G. 1998 Laseroptical investigation of highly preheated combustion with strong exhaust gas recirculation. *27th Symp. Combust.* **27**, 3197–3204.

POPE, STEPHEN B. 2013 Small scales, many species and the manifold challenges of turbulent combustion. *Proc. Combust. Inst.* **34** (1), 1–31.

RICHTER, M., COLLIN, R., NYGREN, J., ALDÉN, M., HILDINGSSON, L. & JOHANSSON, BENGT 2005 Studies of the Combustion Process with Simultaneous Formaldehyde and OH PLIF in a Direct-Injected HCCI Engine. *JSME Int. J. Ser. B* **48** (4), 701–707.

ROSELL, J., BAI, X.-S., SJOHOLM, J., ZHOU, B., LI, Z., WANG, Z., PETERSSON, P., LI, Z., RICHTER, M. & ALDÉN, M. 2017 Multi-species PLIF study of the structures of turbulent premixed methane/air jet flames in the flamelet and thin-reaction zones regimes. *Combust. Flame* **182**, 324–338.

SIDEY, J. A. M., MASTORAKOS, E. & GORDON, R. L. 2014 Simulations of Autoignition and Laminar Premixed Flames in Methane/Air Mixtures Diluted with Hot Products. *Combust. Sci. Technol.* **186** (4-5), 453–465.

SMOOKE, M. D. & GIOVANGIGLI, V. 1991 Formulation of the premixed and nonpremixed test problems. In *Reduc. Kinet. Mech. Asymptot. Approx. Methane-Air Flames* (ed. M. D. Smooke), *Lecture Notes in Physics*, vol. 384, pp. 1–28. Berlin/Heidelberg: Springer Berlin Heidelberg.

SORRENTINO, G., SABIA, P., DE JOANNON, M., CAVALIERE, A. & RAGUCCI, R. 2016 The Effect of Diluent on the Sustainability of MILD Combustion in a Cyclonic Burner. *Flow, Turbul. Combust.* **96** (2), 449–468.

TANAHASHI, M., MURAKAMI, S., CHOI, G.-M., FUKUCHI, Y. & MIYAUCHI, T. 2005 Simultaneous CHOH PLIF and stereoscopic PIV measurements of turbulent premixed flames. *Proc. Combust. Inst.* **30** (1), 1665–1672.

WABEL, T. M., ZHANG, P., ZHAO, X., WANG, H., HAWKES, E. & STEINBERG, A. M. 2018 Assessment of chemical scalars for heat release rate measurement in highly turbulent premixed combustion including experimental factors. *Combust. Flame* **194**, 485–506.

WÜNNING, J. A. & WÜNNING, J. G. 1997 Flameless oxidation to reduce thermal no-formation. *Prog. Energy Combust. Sci.* **23** (1), 81–94.

YAMASHITA, H., SHIMADA, M. & TAKENO, T. 1996 A numerical study on flame stability at the transition point of jet diffusion flames. *26th Symp. Combust.* **26** (1), 27–34.

ZHOU, B., KIEFER, J., ZETTERBERG, J., LI, Z. & ALDÉN, M. 2014 Strategy for PLIF single-shot HCO imaging in turbulent methane/air flames. *Combust. Flame* **161**, 1566–1574.